

Pilot-to-Data Power Ratio in RIS-Assisted Multiantenna Communication

Masoud Sadeghian, *Student Member, IEEE*, Angel Lozano, *Fellow, IEEE*, Gabor Fodor, *Fellow, IEEE*

Abstract—The optimization of the pilot-to-data power ratio (PDPR) is a recourse that helps wireless systems to acquire channel state information while minimizing the pilot overhead. While the optimization of the PDPR in cellular networks has been studied extensively, the effect of the PDPR in reconfigurable intelligence surface (RIS)-assisted networks has hardly been examined. This paper tackles this optimization when the communication is assisted by a RIS whose phase shifts are adjusted on the basis of the statistics of the channels. For a setting representative of a macrocellular deployment, the benefits of optimizing the PDPR are seen to be significant over a broad range of operating conditions. These benefits, demonstrated through the ergodic minimum mean squared error, for which a closed-form solution is derived, become more pronounced as the number of RIS elements and/or the channel coherence grow large.

Index Terms—Multiantenna communication, reconfigurable intelligent surface, pilot power boosting

I. INTRODUCTION

In order to minimize the number of pilot symbol transmissions, and increase their effectiveness, wireless systems can in principle allocate unequal powers to pilot and data symbols, subject to an average power constraint [1, 2]. Indeed, many wireless systems do feature a pilot-to-data power ratio (PDPR) that is not unity, but rather skewed towards the pilots. The 3GPP Long-Term Evolution and New Radio systems, for example, facilitate adjusting the number of pilot symbols and boosting their power [3]. This paper seeks to expand this understanding to the new paradigm in which the communication is assisted by a reconfigurable intelligence surface (RIS).

With strategic RIS placement and phase shift adjustment, a RIS can help overcome the limitations of a weak direct link, facilitating communication in scenarios where it would normally be unfeasible [4]. A RIS drawback, though, is its inability to process received pilot symbols for channel estimation, due to the passive nature of its elements. Estimation of the channels to/from a RIS thus becomes extremely burdensome. To address this issue, some works have attempted to reduce the pilot overhead by grouping the RIS elements [5] (see also [6, 7], which explore the grouping of elements in conjunction with PDPR in single-input single-output RIS-assisted communication). Nevertheless, the system still requires a prohibitively large number of pilot transmissions

[8, 9]. An enticing alternative is to adjust the phase shifts based only on the channel statistics, rather than on its realization. This is sometimes referred to as the two-timescale scheme, in reference to the short-term adaptation of the receiver and the long-term adaptation of the RIS phase shifts [10–13]. The two-timescale approach dramatically shrinks the number of symbols that must be reserved for pilot transmissions, down to the amount required for the receiver to estimate the cascade channel—exactly as in non-RIS-assisted communication. To further minimize the number of pilot symbol transmissions and increase their effectiveness, the optimization of the PDPR emerges as an opportunity.

This paper proposes to jointly configure the PDPR and the RIS phase shifts such that both are based on the two-timescale operation. This configuration problem is cast as an optimization task, with an iterative algorithm proposed in [14] employed for the computation of the RIS phase shifts, while an original closed-form expression is derived for the PDPR. With a view to representing a macrocellular deployment where the RIS is situated above the scattering clutter, the channel between the base station (BS) and the RIS is taken to be line of sight (LOS), while the channel between the RIS and mobile station (MS) exhibits correlated fading. Given this setup, the focus is on the uplink, with minimum mean squared error (MMSE) reception. We hasten to emphasize that the actual MMSE receiver is formulated, rather than the one that would take the channel estimate as exact and then minimize the signal mean-square error under that premise [15]. The two receivers need not coincide, depending on how the channel is estimated and what its statistics are. The RIS phase shifts are, as highlighted earlier, adjusted in a statistical manner. Altogether, this paper contributes to the existing literature by:

- Deriving a closed form for the ergodic MMSE of the actual MMSE receiver in RIS-assisted communication.
- Establishing the optimal PDPR as a function of the fading coherence, the number of antennas at the BS, the number of RIS elements, and the RIS phase shifts.

Through the optimization of the PDPR for the MMSE receiver in practical scenarios with explicit channel estimation, this paper illustrates the feasibility of improving the ergodic MMSE in RIS-assisted communication, with gains of up to 3 dB.

II. SYSTEM MODEL

Consider a single-antenna MS communicating with an N_b -antenna BS, aided by a RIS equipped with N_r elements. Assuming the channel remains constant over a fading coherence period of τ_c symbols, the MS first transmits pilot symbols for

Masoud Sadeghian and Angel Lozano are with the Department of Engineering, Univ. Pompeu Fabra, 08018 Barcelona, Spain ({masoud.sadeghian, angel.lozano}@upf.edu). Gabor Fodor is with the School of Electrical Engineering and Computer Science, KTH Royal Institute of Technology, 10044 Stockholm, Sweden and Ericsson Research, 16480 Stockholm, Sweden. Work supported by the Horizon 2020 MSCA-ITN-METAWIRELESS Grant Agreement 956256, by MICIU under grant CEX2021001195-M, by ICREA, and by the Swedish SSF project SAICOM, Grant No: FUS21-0004.

the purpose of channel estimation, subsequently followed by payload data symbols.

A. Uplink Pilot Signal Model

The pilot symbols conform to a Zadoff-Chu sequence of length τ_p , namely

$$\mathbf{s} = [s_1, s_2, \dots, s_{\tau_p}]^T \in \mathbb{C}^{\tau_p \times 1}, \quad (1)$$

whose entries satisfy $|s_j|^2 = 1$. The observed pilot sequence $\mathbf{Y}_p \in \mathbb{C}^{N_b \times \tau_p}$ at the BS is

$$\mathbf{Y}_p = \alpha \sqrt{P_p} \mathbf{h} \mathbf{s}^T + \mathbf{N}_p, \quad (2)$$

where α represents the large-scale channel gain, P_p is the transmit power over the pilot sequence, and $\mathbf{N}_p \in \mathbb{C}^{N_b \times \tau_p}$ is additive white Gaussian noise (AWGN), with independent entries having variance σ^2 . The RIS becomes crucial when the direct link is weak or obstructed [4, 16]. In this case, the cascade channel $\mathbf{h} \in \mathbb{C}^{N_b \times 1}$ is formed by the RIS reflections, as detailed in Sec. II-C, while the direct link is assumed to be obstructed. Letting $\text{vec}(\cdot)$ denote the column stacking operator,

$$\mathbf{y}_p = \text{vec}(\mathbf{Y}_p) = \alpha \sqrt{P_p} \mathbf{S} \mathbf{h} + \mathbf{n}_p, \quad (3)$$

where $\mathbf{y}_p \in \mathbb{C}^{\tau_p N_b \times 1}$ is the vectorized pilot sequence, $\mathbf{n}_p \in \mathbb{C}^{\tau_p N_b \times 1}$ is the vectorized AWGN, and the semiorthogonal matrix $\mathbf{S} = \mathbf{s} \otimes \mathbf{I}_{N_b} \in \mathbb{C}^{\tau_p N_b \times N_b}$ is defined by means of the Kronecker product.

B. Uplink Data Signal Model

Upon payload data transmission, the observation $\mathbf{y}_d \in \mathbb{C}^{N_b \times 1}$ at the BS is

$$\mathbf{y}_d = \alpha \sqrt{P_d} \mathbf{h} x + \mathbf{n}_d, \quad (4)$$

where $\mathbf{n}_d \sim \mathcal{N}_{\mathbb{C}}(\mathbf{0}, \sigma^2 \mathbf{I}_{N_b})$ is the AWGN, P_d is the transmit power, and x is a unit-variance data symbol.

C. Cascade Channel

The channel between the BS and the RIS, represented by $\mathbf{H} \in \mathbb{C}^{N_b \times N_r}$, is LOS, deterministic and of unit rank. The channel between the MS and the RIS is $\mathbf{h}_r \sim \mathcal{N}_{\mathbb{C}}(\mathbf{0}, \mathbf{C}_r)$, with covariance matrix $\mathbf{C}_r \in \mathbb{C}^{N_r \times N_r}$. This covariance can be learned by empirically averaging signal observations. With the configuration of the RIS specified by the phase-shift matrix $\Psi = \text{diag}(\psi)$, where $\psi = [e^{-j\psi_1}, \dots, e^{-j\psi_{N_r}}]^T$, the cascade channel at the BS from the MS is

$$\mathbf{h} = \mathbf{H} \Psi \mathbf{h}_r. \quad (5)$$

III. CHANNEL ESTIMATION

Given the statistical optimization of the RIS, the cascade channel satisfies $\mathbf{h} \sim \mathcal{N}_{\mathbb{C}}(\mathbf{0}, \mathbf{C})$ with covariance matrix

$$\mathbf{C} = \mathbf{H} \Psi \mathbf{C}_r \Psi^* \mathbf{H}^H. \quad (6)$$

By correlating the observations with the known pilot sequence, the BS can obtain the least square estimate of the cascade channel as

$$\hat{\mathbf{h}} = \frac{1}{\alpha \sqrt{P_p}} (\mathbf{S}^H \mathbf{S})^{-1} \mathbf{S}^H \mathbf{y}_p \quad (7)$$

$$= \mathbf{h} + \frac{1}{\alpha \tau_p \sqrt{P_p}} \mathbf{S}^H \mathbf{n}_p, \quad (8)$$

satisfying $\hat{\mathbf{h}} \sim \mathcal{N}_{\mathbb{C}}(\mathbf{0}, \mathbf{R})$ with

$$\mathbf{R} = \mathbf{C} + \frac{\sigma^2}{\alpha^2 \tau_p P_p} \mathbf{I}_{N_b}. \quad (9)$$

Regardless of the channel estimation method, the formulation of the MMSE receiver depends on the conditional distribution of the cascade channel relative to its estimate. This conditional distribution satisfies [17]

$$\mathbf{h} | \hat{\mathbf{h}} \sim \mathcal{N}_{\mathbb{C}}(\mathbf{D} \hat{\mathbf{h}}, \mathbf{Q}), \quad (10)$$

where $\mathbf{D} = \mathbf{C} \mathbf{R}^{-1}$, and $\mathbf{Q} = \mathbf{C} - \mathbf{C} \mathbf{R}^{-1} \mathbf{C}$.

IV. MMSE RECEIVER

By definition, the MMSE receiver $\mathbf{w} \in \mathbb{C}^{N_b \times 1}$ is given by

$$\mathbf{w} = \arg \min_{\mathbf{g}} \mathbb{E} [|\mathbf{g}^H \mathbf{y}_d - x|^2 | \hat{\mathbf{h}}], \quad (11)$$

and the solution to this minimization is [15]

$$\mathbf{w}^H = \alpha \sqrt{P_d} \hat{\mathbf{h}}^H \mathbf{D}^H \cdot \left(\alpha^2 P_d \left(\mathbf{D} \hat{\mathbf{h}} \hat{\mathbf{h}}^H \mathbf{D}^H + \mathbf{Q} \right) + \sigma^2 \mathbf{I}_{N_b} \right)^{-1}, \quad (12)$$

while the ensuing MMSE is

$$\begin{aligned} \mathbb{E} [|\mathbf{w}^H \mathbf{y}_d - x|^2 | \hat{\mathbf{h}}] &= \alpha^2 P_d \mathbf{w}^H \left(\mathbf{D} \hat{\mathbf{h}} \hat{\mathbf{h}}^H \mathbf{D}^H + \mathbf{Q} \right) \mathbf{w} \\ &\quad - \alpha \sqrt{P_d} \left(\mathbf{w}^H \mathbf{D} \hat{\mathbf{h}} + \hat{\mathbf{h}}^H \mathbf{D}^H \mathbf{w} \right) \\ &\quad + \sigma^2 \mathbf{w}^H \mathbf{w} + 1. \end{aligned} \quad (13)$$

Expecting over the distribution of $\hat{\mathbf{h}}$, the ergodic MMSE emerges (see App. A) as

$$\mathbb{E} [|\mathbf{w}^H \mathbf{y}_d - x|^2] = \mathbb{E} \left[\frac{1}{1 + \rho} \right], \quad (14)$$

where

$$\rho = \hat{\mathbf{h}}^H \mathbf{D}^H \left(\mathbf{Q} + \frac{\sigma^2}{\alpha^2 P_d} \mathbf{I}_{N_b} \right)^{-1} \mathbf{D} \hat{\mathbf{h}}. \quad (15)$$

Using $\mathbf{H} = \sqrt{N_r N_b} \mathbf{u} \mathbf{v}^H$, where \mathbf{u} and \mathbf{v} are the steering vectors at RIS and BS, both of unit norm, the covariance matrix of the cascade channel in (6) can be rewritten as

$$\mathbf{C} = N_r N_b \mathbf{u} \mathbf{v}^H \Psi \mathbf{C}_r \Psi^* \mathbf{v} \mathbf{u}^H \quad (16)$$

$$= \zeta N_r N_b \mathbf{u} \mathbf{u}^H, \quad (17)$$

where $\zeta = \mathbf{v}^H \Psi \mathbf{C}_r \Psi^* \mathbf{v}$ (a positive real number) captures the effect of the RIS phase shifts. The more pronounced the correlation among RIS elements, the stronger this effect. Conversely, in the absence of spatial correlations, the phase shifts become immaterial.

As shown in App. B, ρ in (15) is exponentially distributed with parameter

$$\lambda = \frac{\zeta^2 N_r^2 N_b^2}{\zeta N_r N_b \frac{\sigma^2}{\alpha^2 \tau_p P_p} + \zeta N_r N_b \frac{\sigma^2}{\alpha^2 P_d} + \frac{\sigma^2}{\alpha^2 \tau_p P_p} \frac{\sigma^2}{\alpha^2 P_d}}, \quad (18)$$

which leads to the ergodic MMSE becoming

$$\mathbb{E} \left[\frac{1}{1 + \rho} \right] = \frac{1}{\lambda} e^{\frac{1}{\lambda}} E_1 \left(\frac{1}{\lambda} \right), \quad (19)$$

given the exponential integral $E_1(x) = \int_x^\infty \frac{e^{-t}}{t} dt$. The parameter λ represents the ergodic signal-to-noise ratio at the output of the MMSE receiver, including, through ζ , the gains provided by the RIS phase shifts, as well as the gains from having multiple RIS elements and BS antennas. It can be verified that (19) is a convex function of λ , which can be minimized by optimizing over P_p , P_d , and ζ .

V. IMPACT OF THE PDPR AND RIS PHASE SHIFTS

A. PDPR

The optimization over P_p and P_d capitalizes on the ability of wireless systems to allocate unequal powers to pilot and data symbols within a given power budget, such that

$$\frac{\tau_p}{\tau_c} P_p + \frac{\tau_d}{\tau_c} P_d = P_t, \quad (20)$$

where P_t quantifies the average transmit power constraint on a per-symbol basis, and $\tau_d = \tau_c - \tau_p$ is the number of data symbols within the coherence interval.

Let $\gamma_p = P_p/P_t$ and $\gamma_d = P_d/P_t$ be the pilot and data power ratios relative to the average power. As the cascade channel is rank-1, hence essentially one-dimensional, $\tau_p = 1$ suffices. Then, $\tau_d = \tau_c - 1$ and the power ratios can be seen to satisfy

$$\gamma_d = \frac{\tau_c - \gamma_p}{\tau_c - 1}. \quad (21)$$

Plugging γ_p and γ_d in (18) and letting $\text{SNR} = \alpha^2 P_t / \sigma^2$ denote the per-antenna SNR at the receiver (prior to the MMSE processing) gives

$$\lambda = \frac{\zeta^2 N_r^2 N_b^2 \text{SNR}^2}{\frac{\tau_c^2 + (\tau_c - 2)\tau_c \gamma_p}{\gamma_p(\tau_c - \gamma_p)} \zeta N_r N_b \text{SNR} + \frac{\tau_c^2(\tau_c - 1)}{\gamma_p(\tau_c - \gamma_p)}}. \quad (22)$$

As λ is convex in γ_p , the optimum value for the latter—provided in (23), atop the next page—is found by setting the derivative to zero. For $\text{SNR} \rightarrow 0$, $\gamma_p^* \rightarrow \tau_c/2$, indicating that half of the transmit energy should be injected on the pilot while the rest is spread over the data symbols; this is consistent with standard results in non-RIS-assisted multiantenna communication [18, Ch. 4.8.2]. It follows that the PDPR for vanishing SNR satisfies $\gamma_p^*/\gamma_d^* \rightarrow \tau_c - 1$. Conversely, for $\text{SNR} \rightarrow \infty$,

$$\gamma_p^* \rightarrow \frac{\tau_c}{1 + \sqrt{\tau_c - 1}}, \quad (24)$$

whereby the PDPR satisfies

$$\frac{\gamma_p^*}{\gamma_d^*} \rightarrow \sqrt{\tau_c - 1}. \quad (25)$$

As implied by (25), the peakedness of the PDPR grows with $\sqrt{\tau_c}$ for large τ_c . Only for very large τ_c could this become

Algorithm 1 Computation of RIS phase shifts via DSM

```

1: input:  $\mathbf{G}$  and  $\epsilon$ 
2: output:  $\psi^{(k)}$  and  $\zeta^{(k)} = \psi^{(k)\text{H}} \mathbf{G} \psi^{(k)}$ 
3: initialize  $k = 0$  and set an initial  $\psi^{(0)}$ 
4: compute  $g_{nm} = [\mathbf{G}]_{nm}$ 
5: while  $|\zeta^{(k)} - \zeta^{(k-1)}| > \epsilon$  do
6:   increase  $k$ 
7:   for  $n = 1, \dots, N_r$  do
8:     Update  $\psi_n^{(k)}$  using (28)
9:   end for
10: end while

```

excessive, and in that case the PDPR could be truncated with negligible loss in performance.

Fig. 1 shows the ergodic MMSE as a function of γ_p for different numbers of RIS elements, N_r , with the high-SNR limit in (24) being approached as the number of RIS elements grows large for a given $\zeta N_b \text{SNR}$. The stars indicate the optimal pilot power boosting in (23), while the two vertical lines indicate its low- and high-SNR limits. The solid circles indicate the ergodic MMSE when equal power is allocated to pilot and data symbols, i.e., for $\gamma_p = 1$. As the number of RIS elements increases, the gap between the stars and the solid circles widens, indicating a higher advantage from optimizing the PDPR.

B. RIS Phase Shifts

Since λ is strictly increasing in ζ , due to ζ being positive and real, the optimum phase shifts are those that maximize ζ . Rewriting it as $\zeta = \psi^H \mathbf{G} \psi$, where $\mathbf{G} = \text{diag}(\mathbf{v}^H) \mathbf{C}_r \text{diag}(\mathbf{v})$, the optimization of the RIS phase shifts can be cast as

$$(P1): \max_{\psi} \psi^H \mathbf{G} \psi \quad (26)$$

$$\text{s.t.} \quad |\psi_i| = 1 \quad i = 1, 2, \dots, N_r, \quad (27)$$

whose objective function is quadratic, but whose unit-magnitude constraints are not convex. The optimization problem (P1) was investigated in [14, 19], where dimension-wise sinusoidal maximization (DSM) was identified as an effective solution. This paper applies a modified DSM approach [14]. The phase shift of the n th RIS element, $\psi_n^{(k)}$, is optimized, while keeping the phases of all other elements fixed, leading to

$$\psi_n^{(k)} = \exp \left(\angle \left[\sum_{m=1}^{n-1} \psi_m^{(k)} g_{nm} + \sum_{m=n+1}^{N_r} \psi_m^{(k-1)} g_{nm} \right] \right), \quad (28)$$

where $g_{nm} = [\mathbf{G}]_{nm}$. Algorithm 1 outlines the implementation, starting with an initial $\psi^{(0)}$.

In an isotropic scattering environment, the most unfavorable one for a RIS with statistical phase shifting, the (n, m) th entry of \mathbf{C}_r equals [20]

$$c_{n,m} = \text{sinc} \left(\frac{2 \|\mathbf{u}_n - \mathbf{u}_m\|}{\lambda_c} \right) \quad n, m = 1, \dots, N_r, \quad (29)$$

where \mathbf{u}_n and \mathbf{u}_m are the positions of the n th and m th RIS elements, respectively, and λ_c is the carrier wavelength.

$$\gamma_p^* = \frac{\frac{\tau_c(1-\tau_c)}{\zeta N_r N_b \text{SNR}} - \tau_c + \tau_c \sqrt{\frac{(\tau_c-1)^2}{(\zeta N_r N_b \text{SNR})^2} + \frac{(\tau_c-1)^2 + (\tau_c-1)}{\zeta N_r N_b \text{SNR}}}}{(\tau_c - 2)} \quad (23)$$

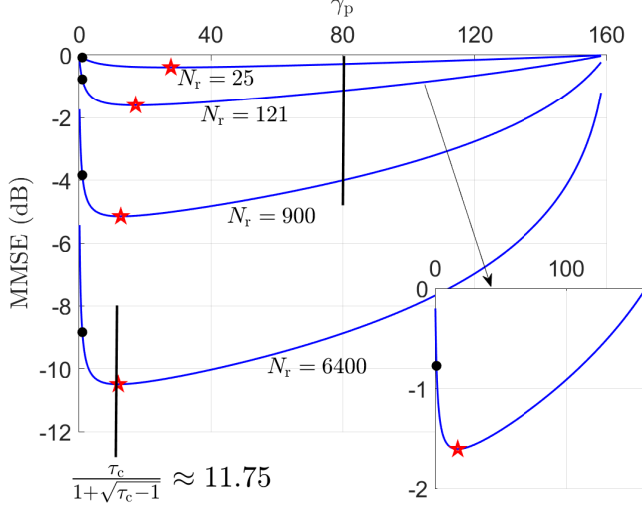


Fig. 1. Ergodic MMSE as a function of $0 < \gamma_p < \tau_c$ for various numbers of RIS elements, $\tau_c = 160$, and $\zeta N_b \text{SNR} = 0$ dB.

Considering a planar square RIS and a BS with $N_b = 10$ antennas arranged as a 2×5 planar array with half-wavelength spacing, Fig. 2 depicts the ergodic MMSE as a function of the number of RIS elements. The spacing between the RIS elements is $\lambda_c/7$ along each dimension, and $\text{SNR} = -10$ dB. When the number of RIS elements is small, increasing it causes λ in (22) to grow quadratically, which leads to a steeper reduction in ergodic MMSE. Conversely, with a large number of RIS elements, the increase in λ becomes linear, causing the ergodic MMSE to decrease more slowly as additional RIS elements are introduced.

VI. CONCLUSION

This paper has shown that a PDPR optimization, even with a suboptimal RIS phase shift configuration such as the one embodied by Algorithm 1, leads to a substantial performance improvement. This advantage increases steadily with the number of RIS elements, as the system is pushed into an effectively higher SNR. The advantage also increases noticeably with the fading coherence, but, even for short coherences, gains of roughly 3 dB can be observed over a broad range of operating conditions of interest for macrocellular systems.

APPENDIX A

From (13), the ergodic MMSE is

$$\mathbb{E}[|w^H y_d - x|^2] = \mathbb{E}_{\hat{h}} \left[1 - 2 \underbrace{\alpha \sqrt{P_d} w^H D \hat{h}}_{\text{term 1}} + \underbrace{\alpha^2 P_d w^H \left(D \hat{h} \hat{h}^H D^H + Q + \frac{\sigma^2}{\alpha^2 P_d} I_{N_b} \right) w}_{\text{term 2}} \right]. \quad (30)$$

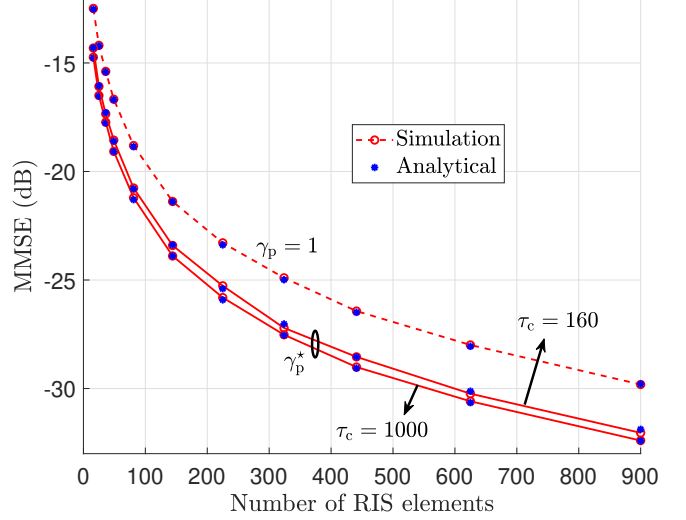


Fig. 2. Ergodic MMSE versus number of RIS elements for two distinct coherence intervals. The dashed line corresponds to $\gamma_p = 1$ (any fading coherence) while the solid lines correspond to the optimal pilot power boosting in (23). Algorithm 1 is used to obtain the RIS phase shifts for both the dashed and solid lines.

Recalling (12), letting $A = Q + \frac{\sigma^2}{\alpha^2 P_d} I_{N_b}$, and applying the Sherman–Morrison formula, term 1 emerges as

$$\begin{aligned} \hat{h}^H D^H \left(D \hat{h} \hat{h}^H D^H + A \right)^{-1} D \hat{h} \\ = \hat{h}^H D^H \left(A^{-1} - \frac{A^{-1} D \hat{h} \hat{h}^H D^H A^{-1}}{1 + \hat{h}^H D^H A^{-1} D \hat{h}} \right) D \hat{h} \end{aligned} \quad (31)$$

$$= \frac{\hat{h}^H D^H A^{-1} D \hat{h}}{1 + \hat{h}^H D^H A^{-1} D \hat{h}} \quad (32)$$

while term 2 becomes

$$\begin{aligned} \hat{h}^H D^H \left(D \hat{h} \hat{h}^H D^H + A \right)^{-1} \left(D \hat{h} \hat{h}^H D^H + A \right) \\ \cdot \left(D \hat{h} \hat{h}^H D^H + A \right)^{-1} D \hat{h} \\ = \hat{h}^H D^H \left(D \hat{h} \hat{h}^H D^H + A \right)^{-1} D \hat{h} \end{aligned} \quad (33)$$

$$= \frac{\hat{h}^H D^H A^{-1} D \hat{h}}{1 + \hat{h}^H D^H A^{-1} D \hat{h}}, \quad (34)$$

which mirrors term 1, whose symmetry simplifies (30) to

$$\mathbb{E}[|w^H y_d - x|^2] = \mathbb{E} \left[\frac{1}{1 + \rho} \right], \quad (35)$$

with $\rho = \hat{h}^H D^H A^{-1} D \hat{h}$.

APPENDIX B

By plugging (17) and simplifying,

$$R^{-1} = \left(\frac{\sigma^2}{\alpha^2 \tau_p P_p} I_{N_b} + \zeta N_r N_b u u^H \right)^{-1} \quad (36)$$

$$= \frac{1}{\zeta N_r N_b} \frac{\zeta N_r N_b \alpha^2 \tau_p P_p}{\sigma^2} \left(\mathbf{I}_{N_b} - \frac{\mathbf{u} \mathbf{u}^H}{1 + \frac{\sigma^2}{\zeta N_r N_b \alpha^2 \tau_p P_p}} \right) \quad (37)$$

$$= \frac{\alpha^2 \tau_p P_p}{\sigma^2} \left(\mathbf{I}_{N_b} - \frac{\zeta N_r N_b \alpha^2 \tau_p P_p}{\zeta N_r N_b \alpha^2 \tau_p P_p + \sigma^2} \mathbf{u} \mathbf{u}^H \right), \quad (38)$$

where (37) follows from the Sherman–Morrison formula. Thus,

$$\mathbf{C} \mathbf{R}^{-1} \mathbf{C} = \frac{\zeta^2 N_r^2 N_b^2 \alpha^2 \tau_p P_p}{\sigma^2} \mathbf{u} \mathbf{u}^H \left(\mathbf{I}_{N_b} - \frac{\zeta N_r N_b \alpha^2 \tau_p P_p}{\zeta N_r N_b \alpha^2 \tau_p P_p + \sigma^2} \mathbf{u} \mathbf{u}^H \right) \mathbf{u} \mathbf{u}^H \quad (39)$$

$$= \frac{\zeta^2 N_r^2 N_b^2}{\zeta N_r N_b + \frac{\sigma^2}{\alpha^2 \tau_p P_p}} \mathbf{u} \mathbf{u}^H, \quad (40)$$

which leads to

$$\mathbf{Q} = \mathbf{C} - \mathbf{C} \mathbf{R}^{-1} \mathbf{C} \quad (41)$$

$$= \frac{\zeta N_r N_b \frac{\sigma^2}{\alpha^2 \tau_p P_p}}{\zeta N_r N_b + \frac{\sigma^2}{\alpha^2 \tau_p P_p}} \mathbf{u} \mathbf{u}^H. \quad (42)$$

After some linear algebra, $\mathbf{D} \mathbf{R}^{1/2} = (\mathbf{C} \mathbf{R}^{-1} \mathbf{C})^{1/2}$, giving

$$\mathbf{D} \mathbf{R}^{1/2} = \sqrt{\frac{\zeta^2 N_r^2 N_b^2}{\zeta N_r N_b + \frac{\sigma^2}{\alpha^2 \tau_p P_p}}} \mathbf{u} \mathbf{u}^H. \quad (43)$$

Applying the Sherman–Morrison formula again,

$$\begin{aligned} & \left(\mathbf{Q} + \frac{\sigma^2}{\alpha^2 P_d} \mathbf{I}_{N_b} \right)^{-1} \\ &= \left(\frac{\zeta N_r N_b \frac{\sigma^2}{\alpha^2 \tau_p P_p}}{\zeta N_r N_b + \frac{\sigma^2}{\alpha^2 \tau_p P_p}} \mathbf{u} \mathbf{u}^H + \frac{\sigma^2}{\alpha^2 P_d} \mathbf{I}_{N_b} \right)^{-1} \quad (44) \\ &= \frac{\alpha^2 P_d}{\sigma^2} \left(\mathbf{I}_{N_b} - \frac{\zeta N_r N_b \frac{\sigma^2}{\alpha^2 \tau_p P_p}}{\zeta N_r N_b \frac{\sigma^2}{\alpha^2 \tau_p P_p} + \zeta N_r N_b \frac{\sigma^2}{\alpha^2 P_d} + \frac{\sigma^2}{\alpha^2 \tau_p P_p} \frac{\sigma^2}{\alpha^2 P_d}} \mathbf{u} \mathbf{u}^H \right), \quad (45) \end{aligned}$$

and altogether

$$\begin{aligned} & \mathbf{R}^{1/2} \mathbf{D}^H \left(\mathbf{Q} + \frac{\sigma^2}{\alpha^2 P_d} \mathbf{I}_{N_b} \right)^{-1} \mathbf{D} \mathbf{R}^{1/2} \\ &= \frac{\zeta^2 N_r^2 N_b^2}{\zeta N_r N_b + \frac{\sigma^2}{\alpha^2 \tau_p P_p}} \frac{\alpha^2 P_d}{\sigma^2} \left(\mathbf{u} \mathbf{u}^H - \frac{\zeta N_r N_b \frac{\sigma^2}{\alpha^2 \tau_p P_p}}{\zeta N_r N_b \frac{\sigma^2}{\alpha^2 \tau_p P_p} + \zeta N_r N_b \frac{\sigma^2}{\alpha^2 P_d} + \frac{\sigma^2}{\alpha^2 \tau_p P_p} \frac{\sigma^2}{\alpha^2 P_d}} \mathbf{u} \mathbf{u}^H \right) \\ &= \underbrace{\frac{\zeta^2 N_r^2 N_b^2}{\zeta N_r N_b \frac{\sigma^2}{\alpha^2 \tau_p P_p} + \zeta N_r N_b \frac{\sigma^2}{\alpha^2 P_d} + \frac{\sigma^2}{\alpha^2 \tau_p P_p} \frac{\sigma^2}{\alpha^2 P_d}}}_{\lambda} \mathbf{u} \mathbf{u}^H. \quad (46) \end{aligned}$$

Plugged into (15), with $\hat{\mathbf{h}} = \mathbf{R}^{1/2} \mathbf{h}_u$ where $\mathbf{h}_u \sim \mathcal{N}_{\mathbb{C}}(\mathbf{0}, \mathbf{I}_{N_b})$, the above evidences that ρ is exponentially distributed with parameter λ .

REFERENCES

- [1] A. Lozano, “Interplay of spectral efficiency, power and Doppler spectrum for reference-signal-assisted wireless communication,” *IEEE Trans. Wireless Commun.*, vol. 7, no. 12, pp. 5020–29, 2008.
- [2] G. Fodor *et al.*, “Performance analysis of a linear MMSE receiver in time-variant Rayleigh fading channels,” *IEEE Trans. Commun.*, vol. 69, no. 6, pp. 4098–4112, 2021.
- [3] H. Elgendi *et al.*, “Uplink performance of LTE and NR with high-speed trains,” in *IEEE Veh. Techn. Conf. (VTC Spring)*, 2021.
- [4] E. Basar *et al.*, “Wireless communications through reconfigurable intelligent surfaces,” *IEEE Access*, vol. 7, pp. 116 753–116 773, 2019.
- [5] Y. Yang *et al.*, “Intelligent reflecting surface meets OFDM: Protocol design and rate maximization,” *IEEE Trans. Commun.*, vol. 68, no. 7, pp. 4522–4535, 2020.
- [6] Y. Li *et al.*, “Joint power allocation and passive beamforming for RIS-assisted wireless energy-constrained systems with multi-user scheduling,” *IEEE Trans. Veh. Technol.*, vol. 72, no. 11, pp. 15 109–15 114, 2023.
- [7] A. Enqvist *et al.*, “Optimizing reconfigurable intelligent surfaces for short transmissions: How detailed configurations can be afforded?” *IEEE Trans. Wireless Commun.*, vol. 23, no. 4, pp. 3377–3391, 2024.
- [8] Z. Wang *et al.*, “Channel estimation for intelligent reflecting surface assisted multiuser communications: Framework, algorithms, and analysis,” *IEEE Trans. Wireless Commun.*, vol. 19, no. 10, pp. 6607–6620, 2020.
- [9] H. Alwazani *et al.*, “Intelligent reflecting surface-assisted multi-user MISO communication: Channel estimation and beamforming design,” *IEEE Open J. Commun. Soc.*, vol. 1, pp. 661–680, 2020.
- [10] K. Zhi *et al.*, “Two-timescale design for reconfigurable intelligent surface-aided massive MIMO systems with imperfect CSI,” *IEEE Trans. Inf. Theory*, vol. 69, no. 5, pp. 3001–3033, 2022.
- [11] Q. Peng *et al.*, “Two-timescale design for reconfigurable intelligent surface-aided URLLC,” *IEEE Trans. Wireless Commun.*, vol. 23, no. 10, pp. 13 664–13 677, 2024.
- [12] Y. Han *et al.*, “Large intelligent surface-assisted wireless communication exploiting statistical CSI,” *IEEE Trans. Veh. Technol.*, vol. 68, no. 8, pp. 8238–8242, 2019.
- [13] A. Kammoun *et al.*, “Asymptotic max-min SINR analysis of reconfigurable intelligent surface assisted MISO systems,” *IEEE Trans. Wireless Commun.*, vol. 19, no. 12, pp. 7748–7764, 2020.
- [14] A. Sirojuddin *et al.*, “Low-complexity sum-capacity maximization for intelligent reflecting surface-aided MIMO systems,” *IEEE Wireless Commun. Lett.*, vol. 11, no. 7, pp. 1354–1358, 2022.
- [15] G. Fodor *et al.*, “On minimizing the MSE in the presence of channel state information errors,” *IEEE Commun. Lett.*, vol. 19, no. 9, pp. 1604–1607, 2015.
- [16] E. Björnson *et al.*, “Reconfigurable intelligent surfaces: A signal processing perspective with wireless applications,” *IEEE Signal Process. Mag.*, vol. 39, no. 2, pp. 135–158, 2022.
- [17] G. Fodor *et al.*, “Performance analysis of block and comb type channel estimation for massive MIMO systems,” in *Proc. 1st Int. Conf. on 5G*, 2014, pp. 62–69.
- [18] R. W. Heath Jr and A. Lozano, *Foundations of MIMO Communication*. Cambridge, U.K.: Cambridge Univ. Press, 2019.
- [19] B. Ning *et al.*, “Beamforming optimization for intelligent reflecting surface assisted MIMO: A sum-path-gain maximization approach,” *IEEE Wireless Commun. Lett.*, vol. 9, no. 7, pp. 1105–1109, 2020.
- [20] E. Björnson and L. Sanguinetti, “Rayleigh fading modeling and channel hardening for reconfigurable intelligent surfaces,” *IEEE Wireless Commun. Lett.*, vol. 10, no. 4, pp. 830–834, 2021.